Nonlinear spectroscopy in the single optical cycle regime

Pshenichnikov, M.S.; Baltuška, A.

Link to publication in University of Groningen/UMCG research database
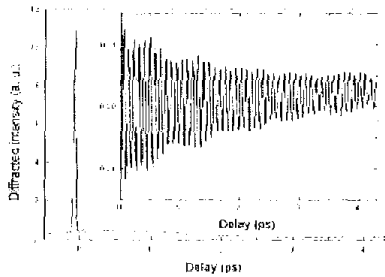
CMK3   Fig. 2.   Result of impulsive stimulated Raman scattering on phonon-polariton in GaP. On the main figure the sharp peak with an FWHM of 36 fs has electronic origin. The signal caused by the polariton is displayed on extended vertical scale in the inset.

Ray tracing calculation indicates that for the set-up shown in Fig. 1, the error originating from the tilt (and curvature) of the pulse fronts of the intersecting pump beams is four times smaller than for a configuration using a conventional beam-splitter for creating the two pump beams. In addition, the compact combination of the transmission grating and the reflective microscope objective results in an improved mechanical stability of the experimental set-up. Further optimization using ray tracing is currently underway.

*Max-Planck-Inst. für Festkörperforschung, Germany*

1. A. Maznev, T.F. Crimmins, K.A. Nelson, "How to make femtosecond pulses overlap," Opt. Lett. **23**, 1378–1380 (1998).
2. Y. Yan and K.A. Nelson, "Impulsive stimulated light scattering. 1. General theory," J. Chem. Phys. **87**, 6240–6265 (1987).

CMK4   **11:45 am**

Nonlinear spectroscopy in the single optical cycle regime

M.S. Pshenichnikov, A. Baltuška, D.A. Wiersma, *Ultrafast Laser and Spectroscopy Lab., Univ. of Groningen, Nijenborgh 4, 9747 AG Groningen, The Netherlands; E-mail: M.S.Pshenichnikov@chem.rug.nl*

The use of extremely short sub-5-fs pulses that became available recently[1-3] provides obvious advantages to a spectroscopic experiment. Next to the very high temporal resolution, the broad bandwidth allows covering an impressive spectral window at once. However, the standard description applicable to multi-cycle pulses becomes questionable for the pulses that consist merely of a couple of optical fringes. The conventionally employed slowly varying envelope approximation,[4] implying that the change of the pulse amplitude on the duration of an optical cycle is negligible compared to the magnitude of the amplitude itself, can no longer be maintained.[5] Furthermore, the phase-matching bandwidth that is limited due to dispersion in the nonlinear medium rapidly gains importance with the broaden-
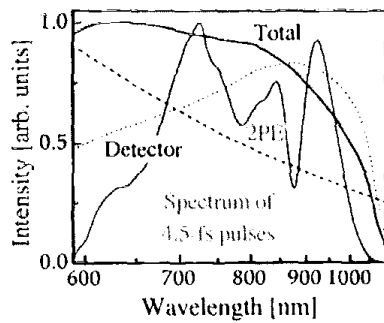
CMK4   Fig. 1.   Spectral filtering effect in photon echo experiment in water. The spectral filter calculated for two-pulse photon echo is shown by a dashed curve while the dotted curve depicts the typical spectral sensitivity of a silicon photodiode. The total spectral filter is given by a solid curve. The thickness of the water layer is taken 100 µm and the intersection angles of the beams are 4°. Shaded contour represents the spectrum of 4.5-fs pulses for a comparison. Note that the overall spectral filter is nearly flat up to 900 nm due to the photo-detector sensitivity balancing off the more efficient generation of the nonlinear signal at higher frequencies.

ing of the pulse spectrum. Another point of serious concern is the frequency-dependent variation in the sensitivity of the photodetector employed to register the signal generated in the nonlinear process. In combination, the above listed features of an experiment with broadband pulses result in what is known as a spectral-filter effect.[6] On top of that, artificial lengthening of the observed time dependencies is a direct consequence of the noncollinear geometry employed in experiments.

In this contribution we present a theoretical analysis in which the frequency- and time-domain formalism of ultrafast nonlinear spectroscopy is thoroughly reexamined. The complete expressions valid even for single-cycle-pulse applications are derived for the nonlinear signal in the frequency and time domains. We also assert that the influence of geometrical delay smearing does not introduce a significant distortion of the observed traces provided that the geometry is carefully optimized. The derived formalism is applied to photon-echo spectroscopy on the hydrated electron with 5-fs pulses.

We consider the case of noncollinear geometry in which three beams intersect at a small angle in nonlinear medium. A typical equation that governs propagation of the fourth, signal, field can be obtained directly from Maxwell's equations:

$$\frac{\partial}{\partial z} E_4(z,\Omega) = i\frac{c\mu_0\Omega}{2n(\Omega)} \int\int d\omega' d\omega'' \bar{\chi}^{(3)}(\Omega; -\omega',\omega'',\Omega - \omega' + \omega')$$

$$\times E_1^*(z,\omega') E_2(z,\omega') E_3(z,\Omega - \omega' + \omega') \exp\left(i\Delta k_z(\Omega,\omega',\omega')z\right.$$

$$\left. - i\omega't_{12} - i(\Omega - \omega' + \omega')t_{13})d\omega' d\omega' \quad (1)$$

where E_i stands for electric fields, $\bar{\chi}^{(3)}$ is the third-order susceptibility, the phase mismatch is denoted as $\Delta k_z(\Omega, \omega', \omega'') = -k_{1z}(\omega') +$
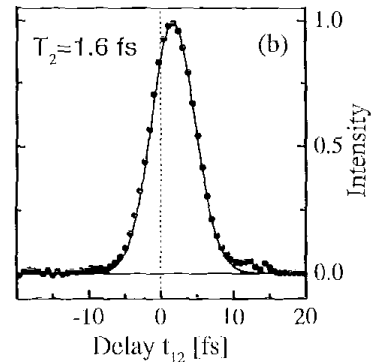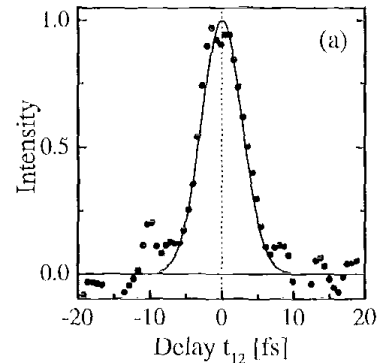
CMK4   Fig. 2.   Results of two-pulse photon echo experiments on water alone (a) and hydrated electrons (b). Circles represent experimental data points and solid curves show fits to the data.

$k_{2z}(\omega'') + k_{3z}(\Omega - \omega'' + \omega'') - k_{4z}(\Omega)$, t_{12} and t_{13} are delays between pulses E_1-E_2 and E_1-E_3, respectively. Equation (1) is valid for optical pulses electric field of which consists of a single cycle at the optical frequency.[7,8]

The spectral filtering effect in the case of two-pulse photon echo experiment ($t_{23} = 0$) is illustrated in Fig. 1 where the frequency-dependent conversion efficiency is shown against the spectral content of the pulse. The spectral window is mostly determined by the self-steepening effect (Ω-term in Eq. (1). The taking into account of a typical spectral sensitivity of a silicon photodiode results in nearly frequency-independent dependence throughout most of the spectrum of a 4.5-fs pulse. This is practically important to justify the use of less cumbersome spectrally unresolved detection of photon echo signals. Note that similar calculations should be employed to optimize the experimental configuration for any third-order spectroscopic experiment that utilizes laser pulses shorter than 10 fs.

Figures 2(a) and 2(b) present the two-pulse photon echo signals obtained from the water and electrons solvated in water,[9] respectively.

A minute difference in the widths of these two traces suggests that the electronic dephasing of the hydrated electrons is extremely fast. The finite population lifetime of the electrons in the excited state causes the delay of the echo trace in Fig. 2(b). The best fit to the experimental data yields the dephasing time of $T_2 = 1.6$ fs. With this value, we successfully modeled the absorption spectrum of the hydrated electrons by an extended Lorentzian line shape,[8] which indicates the breakdown of the rotating wave approximation (RWA).[4]

1. A. Baltuška, et al., Opt. Lett. **22**, 102–104 (1997).
2. M. Nisoli, et al., Opt. Lett. **22**, 522–524 (1997).
3. A. Shirakawa, et al., Appl. Phys. Lett. **74**, 2268 (1999).
4. For example, L. Allen and J.H. Eberly, *Optical resonance and two-level atoms* (Dover publications, New York, 1987).
5. T. Brabec, F. Krausz, Phys. Rev. Lett. **78**, 3282 (1997).
6. A. Baltuska, M.S. Pshenichnikov, D.A. Wiersma, IEEE J. Quantum Electron. **35**, 459 (1999).
7. P.V. Mamyshev and S.V. Chernikov, Opt. Lett. **15**, 1076 (1990).
8. A. Baltuška, M.F. Emde, M.S. Pshenichnikov, D.A. Wiersma, J. Phys. Chem., to be published (1999).
9. C. Silva, et al., Phys. Rev. Lett. **80**, 1086 (1998); M. Emde, et al., Phys. Rev. Lett. **80**, 4645 (1998).

CML

10:15 am–11:45 am
Room 270–276

Polarization Mode Dispersion

Fred L. Heismann, *Tyco Submarine Systems Ltd., USA, Presider*

CML1   **10:15 am**

Polarization mode dispersion in optical communication systems

Curtis R. Menyuk, *Univ. of Maryland–Baltimore Campus, 1000 Hilltop Cir., Baltimore MD 21250, USA*

Polarization mode dispersion (PMD) has become one of the major barriers to achieving single-channel data rates of 10 Gbits/sec and beyond in optical communications systems. In this tutorial, the physical origins of birefringence and PMD are first reviewed. The effects of first-, second-, and higher-order PMD are next elucidated. Finally, PMD compensators and emulators are described. In particular, the need for physically realistic emulators in order to realistically evaluate the effects due to PMD and compensators is emphasized.

CML2   **10:15 am**

PMD probability distribution for arbitrary distances

Jianke Yang, William L. Kath,* Curtis M. Menyuk,** *Department of Mathematics and Statistics, Univ. of Vermont, Burlington, Vermont 05401, USA; E-mail: jyang@emba.uvm.edu*

Polarization mode dispersion (PMD) is caused by the random birefringence present in optical fibers. It can lead to pulse spreading and depolarization, and is detrimental to system performance. As transmission rates continue to increase, PMD has become a major impairment, thus motivating extensive experimental and theoretical study over the past few years.

PMD is characterized by a three-component dispersion vector Ω. Its magnitude $|\Omega|$ gives the differential group delay (DGD) between the principle states, and its direction gives the orientation of the principle states of polarization on the Poincaré sphere at the output. For short distances, PMD is deterministic, and the DGD distribution is a δ-function. For long distances, previous work assuming weak or completely randomizing birefringence models has led to a Maxwellian DGD distribution.[1,2] This long-distance result has been confirmed by numerous numerical and experimental studies. However, there has been as yet no analytic demonstration of this fact assuming a realistic model of the birefringence variation in the fiber. More importantly, there have been no careful studies of how long it takes to reach the asymptotic distribution. This may be important for calculating the penalties due to PMD in the transient regime, because the usual assumption that the distribution is Maxwellian may be erroneous.

In this work, we calculate the DGD distribution in the intermediate distance regime. We begin with the basic dynamical equation for dispersion vector Ω[1]:

$$\frac{\partial \Omega(z,\omega)}{\partial z} = \frac{\partial W(z,\omega)}{\partial \omega} + W(z,\omega)$$

$$\times \Omega(z,\omega), \qquad (1)$$

where the vector W represents the local birefringence in the fiber. We choose a simple realistic birefringence model (the first model of Wai and Menyuk[3]), where the fiber is assumed to have linear birefringence of fixed strength $2b$, but where the birefringence orientation is assumed to be driven by a white noise process. In other words, $W = (2b \cos\theta, 2b \sin\theta, 0)$, and $d\theta/dz = g_0(z)$, where $\langle g_0(z) \rangle = 0$, and $\langle g_0(z)g_0(z') \rangle = \sigma^2 \delta(z - z')$. The parameter σ^2 is related to the fiber correlation length h_{fiber} by the equation $\sigma^2 = 2/h_{\text{fiber}}$. To help simplify the analysis, we employ two variable transformations, $\Omega = R_1(z)\Omega$, and $\hat{\Omega} = R_2(z)\Omega$. Here the matrix R_1 represents a rotation through an angle θ in the (Ω_1, Ω_2) plane, while R_2 is a rotation through an angle $2bz$ in the (Ω_2, Ω_3) plane. Physically, Ω is the dispersion vector measured in terms of local birefringence axes, and $\hat{\Omega}$ is the dispersion vector measured relative to axes rotated by the birefringence. Note that $|\Omega|$ is invariant under these rotations.

We restrict ourselves to the physically important case where the fiber correlation length
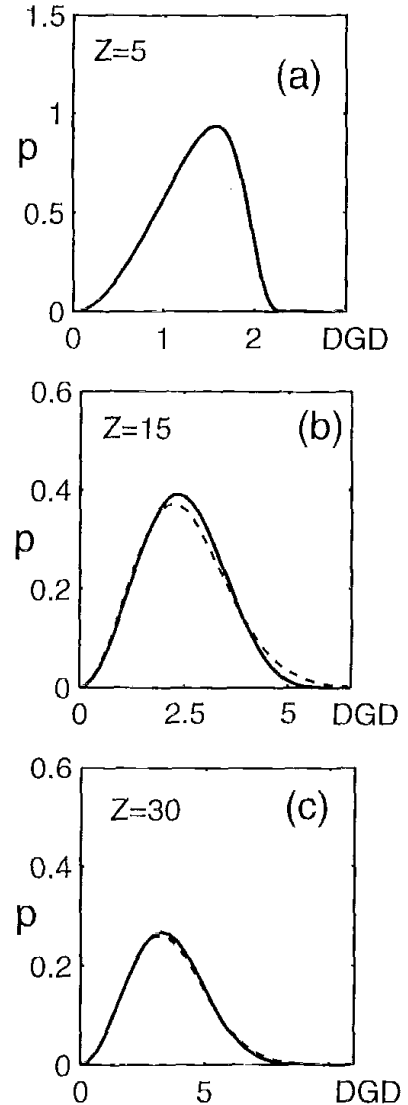
CML2   Fig. 1. Probability distribution p of the differential group delay at various distances. Here $Z = 1$ corresponds to one fiber correlation length, and the DGD unit is $1/4b'h_{\text{fiber}}$. The dotted lines in (b) and (c) are Maxwellian distributions for comparison.

h_{fiber} is much larger than the beat length π/b. In this case, the Fokker–Planck for Ω can be averaged over the rapid birefringence rotation, and the probability density function P for Ω satisfies the following reduced equation[4,5]:

$$\frac{\partial P}{\partial Z} = \frac{1}{2}\left[\left(\bar{\Omega}_1 \frac{\partial}{\partial \bar{\Omega}_2} - \bar{\Omega}_2 \frac{\partial}{\partial \bar{\Omega}_1}\right)^2 + \left(\bar{\Omega}_1 \frac{\partial}{\partial \bar{\Omega}_3}\right.\right.$$

$$\left.\left. - \bar{\Omega}_3 \frac{\partial}{\partial \bar{\Omega}_1}\right)^2\right]P - \frac{1}{2}\frac{\partial P}{\partial \bar{\Omega}_1}. \qquad (2)$$

Here $Z \equiv z/h_{\text{fiber}}$, and $\bar{\Omega}_k \equiv \Omega_k/4b'h_{\text{fiber}}$ ($k = 1$, 2, 3) are dimensionless variables, and the derivative in b' is with respect to frequency. For a typical PMD coefficient 1ps/$\sqrt{\text{km}}$ and fiber correlation length 50 m, the DGD unit ($4b'h_{\text{fiber}}$) is approximately 0.32 ps. It is important to note, however, that Eq. (2) no longer has any free parameters. Thus, the